RESEARCH ARTICLE

Check for updates

Significance of Riga Plate on Marangoni Convective Flow of Casson Hybrid Nanofluid over a Stretching/Shrinking Sheet with Suction and Darcy-Forchheimer Effects

Waqas Ahmad[1,*]

[1] Department of Physical and Numerical Sciences, Qurtuba University of Science and Information Technology, Peshawar 25100, KP, Pakistan

Abstract

This study investigates the heat transfer and Marangoni convection flow of a hybrid Al_2O_3-Cu/water nanofluid over a stretching/shrinking sheet. Surface tension-driven thermal Marangoni convection arises from the wall temperature gradient. The novel aspects include the combined effects of a Riga plate, thermal radiation, the Darcy–Forchheimer model, and Casson fluid characteristics. The Riga plate, comprising magnets and electrodes, generates a Lorentz force influenced by the fluid's vertical electrical conductivity. Similarity transformations convert the governing partial differential equations into ordinary differential equations, which are numerically solved using MATLAB's bvp4c solver. Results show that increasing the Marangoni convection and surface movement parameters enhances the velocity profile while reducing the temperature distribution. Conversely, higher porous medium and Casson parameters decrease both velocity and temperature profiles. The suction parameter reduces the velocity profile while significantly enhancing the Nusselt number by thinning the thermal boundary layer. Streamline and isotherm plots are presented for various parameters. Additionally, the skin friction coefficient and Nusselt number are discussed. These findings hold promise for industrial and medical applications, including biomedical device design, targeted drug delivery, and wastewater treatment.

Keywords: darcy-forchheimer, riga plate, casson fluid, marangoni convection, joule heating, stretching/shrinking sheet.

Subscript	Description
0	Reference/initial condition
w	Wall surface condition
f	Base fluid (water)
∞	Ambient condition (at $y \to \infty$)
hnf	Hybrid nanofluid (Al_2O_3-Cu/water)

Submitted: 13 November 2025
Accepted: 27 April 2026
Published: 30 April 2026

Vol. 2, **No.** 2, 2026.
10.62762/IJTSSE.2026.316433

***Corresponding author:**
Waqas Ahmad
waqas64065@gmail.com

Citation
Ahmad, W. (2026). Significance of Riga Plate on Marangoni Convective Flow of Casson Hybrid Nanofluid over a Stretching/Shrinking Sheet with Suction and Darcy-Forchheimer Effects. *International Journal of Thermo-Fluid Systems and Sustainable Energy*, 2(2), 30–50.

Symbol	Description
u, v	Fluid velocity components (m/s)
x, y	Cartesian coordinates
C	Surface movement parameter
C_p	Specific heat (J·kg^{-1}·K^{-1})
Ma	Marangoni convection parameter
Ec	Eckert number
β_0	Casson parameter
Fr	Darcy-Forchheimer number
k	Porous medium parameter
S	Suction parameter
M	Magnetic parameter
Nu_x	Nusselt number
Pr	Prandtl number
q_r	Thermal radiation heat flux (W·m^{-2})
λ	Stretching/shrinking parameter
T	Fluid temperature (K)
Rd	Thermal radiation parameter
q	Modified Hartmann number
T_w	Surface temperature (K)
Re	Reynolds number
Q	Heat source/sink parameter
Re_x	Local Reynolds number
C_f	Skin friction coefficient
T_∞	Ambient temperature (K)

Abbreviation	Description
PDEs	Partial differential equations
ODEs	Ordinary differential equations
BVP	Boundary value problem
BVPs	Boundary value problems
BCs	Boundary conditions
BL	Boundary layer
BLT	Boundary layer theory
CBLT	Convective boundary layer theory
MHD	Magnetohydrodynamics
HNF	Hybrid nanofluid
NF	Nanofluid
DF	Darcy–Forchheimer
SP	Stagnation point
SPF	Stagnation point flow
RK-IV	Fourth-order Runge-Kutta method
HAM	Homotopy analysis method

Greek letter	Physical meaning
k	Thermal conductivity
ϕ	Nanoparticle volume fraction
η	Non-dimensional similarity parameter
μ	Dynamic viscosity
v	Kinematic viscosity
$(\rho C_p)_f$	Heat capacitance of base fluid
ρ	Density of fluid
$\theta(\eta)$	Dimensionless temperature
ε	Heat capacity ratio

1 Introduction

When the surface tension of a liquid-liquid or liquid-air interface changes in response to concentration or temperature variations, the Marangoni convective transport process is frequently observed. The study of Marangoni flow has attracted considerable interest due to its numerous applications in semiconductor manufacturing, thin-film stretching, materials science, melting processes, nuclear reactors, silicon wafers, welding, nanotechnology, crystal growth, and soap films. Two forms of Marangoni effects are typically distinguished: the solutal Marangoni effect (EMS) and the thermal Marangoni effect (EMT). EMT arises from temperature differences and heat sources that destabilize the interfacial region, while EMS results from an imbalance in cross-surface adsorption caused by chemical reactions and concentration gradients.

Wahid et al. [1] examined the Marangoni flow of hybrid nanofluids (HNFs) across a permeable disk embedded in a porous medium, using water as the base fluid, alumina at a 1% volume fraction, and copper with volume fractions ranging from 0.01% to 1%. Abbas et al. [2] numerically investigated the thermal and magnetic behavior of thermophoretic particles suspended in a dusty tangent hyperbolic nanofluid under magneto-Marangoni convection, employing the RKF-45th-order shooting method. Their findings indicated that as the Marangoni convection parameter increases, the velocity profiles rise while the temperature distributions drop. Elbashbeshy et al. [3] studied Marangoni boundary layer flow as heat moves down an inclined disk through a porous medium, obtaining numerical results using the fourth-order Runge–Kutta (RK-4) method. Agrawal et al. [4] analyzed the effects of thermal radiation, heat sources, and sinks on magneto-Marangoni flow of Al_2O_3 nanofluids over a stretched surface embedded in a porous medium, solving the model numerically via the RK-IV method with shooting and similarity transformations.

While the aforementioned studies have examined Marangoni flows under various physical conditions, the combined influence of a Riga plate, Darcy–Forchheimer porous medium, and Casson rheology on the Marangoni convection of a hybrid nanofluid over a stretching/shrinking sheet has not yet been investigated. This existing research gap provides the main motivation for the present study. Choi [5] first introduced the concept of nanofluids, which consist of nanoparticles uniformly dispersed in a conventional base fluid. Such fluids have been demonstrated to exhibit superior thermal conductivity and enhanced heat transfer performance compared with traditional heat transfer fluids [6, 7]. Sohail et al. [8] provided insights into improving heat transfer processes and fluid behavior over stretching surfaces, contributing to the fundamental understanding of nanofluid dynamics. Jahnavi et al. [9] presented an overview of nanofluid production, mathematical modeling, and applications. Zangooee et al. [10] investigated how non-uniform magnetohydrodynamics (MHD) affect the flow of a three-dimensional hybrid nanofluid over a rapidly stretching and contracting surface. Waseem et al. [11] numerically simulated heat generation, thermal radiation, and thermal transport in water-based nanoparticles. Algehyne et al. [12] examined the flow of a hybrid nanofluid over a stretched, convectively heated surface with suction/injection, non-linear thermal radiation, MHD properties, and electrical conductivity.

The development of hybrid nanofluids aimed to further enhance heat transfer efficiency for various thermal applications. This well-studied class of fluids consists of multiple solid components dispersed in a conventional fluid. The properties of HNFs, including viscosity, specific heat, thermal conductivity, density, and heat transfer, are of particular interest for use in heat exchangers, where increased thermal conductivity improves heat transmission [13]. Further research is needed to fully understand the combinations of different hybrid nanoparticles, their stability, mixing ratios, and the mechanisms that enhance heat transfer. Most experimental and numerical data indicate that hybrid nanofluids are effective working fluids. Sharma et al. [14] studied slip and MHD hybrid nanofluid flow with non-linear thermal radiation over an exponentially stretching/shrinking sheet with a non-uniform heat source/sink. Dandu et al. [15] examined the influence of chemical reactions and thermal radiation on Casson hybrid nanofluid flow through a porous medium, considering thermophoresis, Brownian motion, and mixed convection instability over a stretched sheet.

The Riga plate generates a Lorentz force that drives flow over the plate, though this effect decays rapidly. It is an effective tool for preventing boundary layer separation and reducing turbulence by creating crossed magnetic and electric fields on a flat surface. Abbas et al. [16] examined the effect of a non-uniform heat source on the three-dimensional flow of nanoparticles with various base fluids over a Riga plate, numerically investigating Marangoni convective flow of gyrotactic microorganisms in a dusty Jeffrey hybrid nanofluid using the RKF-45th-order solve. They reported that a 10% increase in the Marangoni convection parameter raises heat and mass transfer rates by 9% and 7.15%, respectively. Turkyilmazoglu [17] obtained exact solutions for boundary layer flow over a Riga plate. Otman et al. [18] performed a mathematical analysis of mixed convective stagnation point flow with aggregation and Joule heating over an extended porous Riga plate, solving the model numerically in Mathematica using the RK-IV shooting method. They found that skin friction and heat transfer increase with suction, and the temperature and Nusselt number rise with the heat source parameter. Hussain et al. [19] studied nanofluid flow over a nonlinearly stretching Riga plate of varying thickness, accounting for Joule heating and velocity slip. Their results indicated that the velocity profile improves with the modified Hartmann number, while the thickness parameter has opposite effects on temperature and velocity, and the heat transfer coefficient decreases with increasing thermophoresis and Brownian motion parameters. Eldabe et al. [20] investigated the boundary layer flow of a magnetohydrodynamic micropolar nanofluid over a vertically stretching Riga plate with Joule heating and viscous dissipation, showing that the velocity decreases as the magnetic field parameter increases. Turkyilmazoglu [21] presented two models and new time-dependent solutions for unsteady heat and fluid flow induced by stretching or shrinking sheets. Jawad et al. [22] numerically simulated thermal radiative flow of a tangent hyperbolic nanofluid over a Riga plate in the presence of Joule heating.

Eladeb et al. [23] studied the effects of thermal radiation and bioconvection on radiative Darcy–Forchheimer hybrid nanofluid flow over a contracting and expanding surface, noting that an aligned magnetic field reduces fluid velocity while a spinning component increases it. Gautam et al. [24] illustrated the roles of activation energy and binary chemical reactions in Williamson MHD nanofluid flow in a Darcy–Forchheimer porous medium over an expanding sheet of variable thickness. Ullah et al. [25] examined quadratic convection-driven Darcy–Forchheimer hybrid nanofluid flow through a stretched tube. Muhammad et al. [26] highlighted the significance of carbon nanotube-based nanofluids in Darcy–Forchheimer porous media. Alqahtani et al. [27] studied MHD Casson Darcy–Forchheimer heat and mass transfer over an exponential stretching sheet using a hybrid nanofluid, finding that the energy transfer rate is significantly reduced by suction and Darcy–Forchheimer effects but enhanced by thermal radiation and heat absorption. Usman et al. [28] investigated MHD hybrid nanofluid flow over an exponential stretchable sheet with Darcy–Forchheimer effects and slip conditions. Rasool et al. [29] analyzed Darcy–Forchheimer flow of a Casson-type MHD nanofluid under non-linear stretching conditions using the RK-IV method, showing that temperature increases with thermophoresis and Brownian motion, while mass transfer, heat transfer, and wall drag decrease with increasing slip parameter. Ali et al. [30] studied radiative cross-ternary hybrid nanofluid flow over a stretched cylinder in a Darcy–Forchheimer porous medium with entropy minimization. Many other researchers have also considered Darcy–Forchheimer effects [31–36].

Suction is a boundary layer management technique that reduces fluid velocity and flow rate by inducing a pressure drop at the flow system exit. It plays a crucial role in the design and operation of many devices, particularly microfluidic and nanofluidic systems. Interest in suction effects in hybrid nanofluid flow has recently increased, as nanoparticles significantly alter fluid properties and behavior. Sindhu et al. [37] demonstrated that both water-based mono and hybrid nanofluids (Cu and Al_2O_3) support Darcy–Forchheimer flow with injection and suction over a stretched surface. Zainal et al. [38] examined time-dependent suction and MHD effects in ternary hybrid nanofluid flow over a stretching surface. Jaafar et al. [39] studied MHD stagnation point flow of a moving permeable flat surface, transforming the governing unsteady equations into similarity forms for numerical and analytical analysis. Kandasamy and Zainal et al. [40] investigated the effects of non-linear thermal radiation on double-diffusive mixed convective stagnation point flow of a tangent hyperbolic nanofluid with injection and suction. Shaikh et al. [41] presented a quantitative analysis of flow characteristics and heat transfer in ternary water-based nanofluids under suction/injection and stretching/shrinking sheet conditions. Maiti and Mukhopadhyay [42] studied MHD hybrid nanofluid boundary layer flow through a divergent channel with mass injection and suction, noting two solutions for each suction value but only one for injection. Many researchers have also considered suction effects [43–45].

In this study, we perform for the first time a numerical analysis of Marangoni convective Darcy–Forchheimer Casson hybrid nanofluid flow over a stretching/shrinking sheet with a Riga plate under gravitational effects. A major highlight is the investigation of Marangoni convection and suction effects, which remain relatively underexplored in hybrid nanofluid dynamics. The results hold promise for various industrial and medical applications, including biomedical device design, targeted drug delivery, and wastewater treatment. The hybrid nanofluid is modeled by dispersing Al_2O_3 and Cu nanoparticles in water as the base fluid. The boundary value problem is successfully solved using a shooting method combined with MATLAB's bvp4c solver. The findings indicate that as the Marangoni convection and surface movement parameters increase, the velocity profiles rise while the temperature distributions fall. Conversely, the velocity and temperature profiles decrease with increasing porous medium, suction, and Casson parameters. Streamline and isotherm plots are presented for various parameters. Furthermore, numerical results for the skin friction coefficient and Nusselt number are discussed.

2 Problem Formulation

This study examines the impacts of a Riga plate, Suction, Marangoni convection, Joule heating, and Darcy–Forchheimer porous media effects on a continuous 2-dimensional flow and heat transfer across a stretched surface using a Casson HNF. The hybrid nanofluid's constituent copper (Cu) and aluminum (Al_2O_3) nanoparticles were selected due to their proven effectiveness and thermal conductivity in industrial environments. The base fluid is water (H_2O), in which these nanoparticles are evenly distributed, producing a constant, homogenous, and incompressible flow. In addition, Figure 1, which shows the Cartesian coordinate system, has the x- and y-axes parallel to and normal to the surface. According to the directional arrows in Figure 1, where the starting velocity is given by $u_w(x) = ax$, the surface movement parameter c describes the flow behavior: for $c < 0$, the surface is permeable stretching; for $c > 0$, it is permeable shrinking; and at $c = 0$, the surface remains stationary. The ambient temperature T_∞, surface temperature $T_w(x)$, and characteristic sheet length L are related by the formula

$$T_w(x) = T_\infty + T_0\left(\frac{x}{L}\right).$$

In addition, the temperature-dependent variation in surface tension is linear

$$\delta = \delta_0\left[1 - \bar{\delta}(T - T_\infty)\right].$$

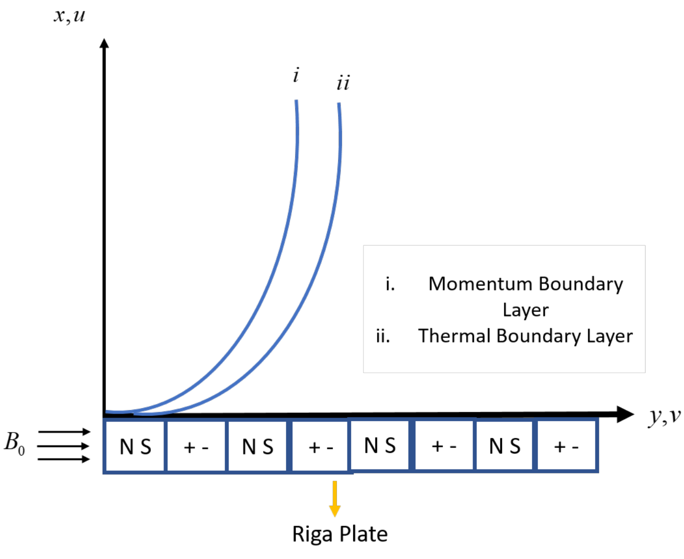

Figure 1. Geometry of flow.

Khashi'ie et al. [46], Alabdulhadi et al. [47], and Jawad et al. [22] incorporates the MHD effect and the governing equations for HNFs, and is dictated by Marangoni boundary layer flow and heat transfer models.

$$\frac{\partial u}{\partial x} + \frac{\partial v}{\partial y} = 0, \tag{1}$$

$$\begin{aligned} u\frac{\partial u}{\partial x} + v\frac{\partial u}{\partial y} &= \frac{\mu_{hnf}}{\rho_{hnf}}\left(1 + \frac{1}{\beta}\right)\frac{\partial^2 u}{\partial y^2} \\ &+ \frac{1}{8}\frac{\pi J_0 \bar{M}_0}{\rho_{hnf}}\exp\left(-\frac{y\pi}{\alpha_1}\right) \\ &- \frac{\mu_{hnf}}{\rho_{hnf} k}u - \frac{c_b}{x\sqrt{k}}u^2, \end{aligned} \tag{2}$$

$$\begin{aligned} \frac{\partial T}{\partial x} + v\frac{\partial T}{\partial y} &= \frac{k_{hnf}}{(\rho C_p)_{hnf}}\frac{\partial^2 T}{\partial y^2} \\ - \frac{\partial q_r}{(\rho C_p)_{hnf}\,\partial y} &+ \frac{Q}{(\rho C_p)_{hnf}}(T - T_\infty) + \frac{\sigma_{hnf}}{(\rho C_p)_{hnf}}B_0^2 u^2, \end{aligned} \tag{3}$$

along with boundary conditions:

$$\begin{cases} v = v_0, \quad T = T_w, \quad \mu_{hnf}\dfrac{\partial u}{\partial y} = \lambda\dfrac{\partial \delta}{\partial T}\dfrac{\partial T}{\partial x}, & \text{at } y = 0, \\ u \to 0, \quad T \to T_\infty, & \text{as } y \to \infty, \end{cases}$$
$$\text{where } \delta = \delta_0\left(1 - \delta(T - T_\infty)\right). \tag{4}$$

Equation 1 shows the continuity equation. The convective terms are shown in Equation 2's L.H.S., while the viscous dissipation with Casson fluid is shown in the first term of R.H.S., the Riga plate in the second term, and the Darcy-Forchheimer term in the third term. Joule heating is represented by the final term of R.H.S. in equation 3, whereas heat source/sink is represented by the second last term, also 2^{nd} terms is thermal radiation, and first term is diffusion term. The velocity components in this investigation are represented by u & v along the x & y-axis. A constant magnetic field B_0, Fluid temperature T, and surface tension temperature gradient denoted by the coefficient γ_T are all included in the model. $v_0 = \sqrt{a v_f} S$ is the formula for the constant mass flow velocity v_0, where a positive v_0 denotes suction and a negative v_0 denotes injection. The term v_0 is replaced by the suction component S when the boundary conditions are converted into non-dimensional form, as equation (4) explains.

In Eq. (3), $q_r = -\frac{4\delta_0}{3k}\frac{\partial T^4}{\partial y}$ provided that there is a sufficiently small temperature differential inside the flow domain, therefore, T^4 can be extended about $T - T_\infty$ in a reasonable manner by using the Taylor series and ignoring the bigger terms results in:

$$T^4 \cong T_\infty^4 + 4T_\infty^3(T - T_\infty), \tag{5}$$

The reduced form of T^4 and differentiating it w.r.t. y, we get:

$$\frac{\partial q_r}{\partial y} = -\frac{16\delta_0}{3k_0} T_\infty^3 \frac{\partial^2 T}{\partial y^2}. \tag{6}$$

Introducing Eq. (7) in Eq. (3) yield to:

$$u\frac{\partial T}{\partial x} + v\frac{\partial T}{\partial y} = \frac{k_{hnf}}{(\rho C_p)_{hnf}} \frac{\partial^2 T}{\partial y^2} + \frac{16\delta_0 T_\infty^3}{(\rho C_p)_{hnf}\, 3k_0} \frac{\partial^2 T}{\partial y^2} + \frac{Q_0}{(\rho C_p)_{hnf}}(T - T_\infty) + \frac{\sigma_{hnf}}{(\rho C_p)_{hnf}} B_0^2 u^2. \tag{7}$$

Equation of continuity is trivially satisfied.

$$\frac{\mu_{hnf}/\mu_f}{\rho_{hnf}/\rho_f}\left(1+\frac{1}{\beta}\right) f''' - (f')^2 + ff'' + \frac{\rho_f}{\rho_{hnf}} q \exp(-d\eta) - \frac{\mu_{hnf}/\mu_f}{\rho_{hnf}/\rho_f} K f' - Fr f'^2(\eta) = 0, \tag{8}$$

$$\frac{k_{hnf}/k_f}{Pr\,(\rho C_p)_{hnf}/(\rho C_p)_f}\theta'' + \frac{(\rho C_p)_f}{Pr\,(\rho C_p)_{hnf}} \frac{4Rd}{3}\theta'' + f\theta' - 2f'\theta + \frac{(\rho C_p)_f}{(\rho C_p)_{hnf}} Q\theta + \frac{\sigma_{hnf}/\sigma_f}{(\rho C_p)_{hnf}/(\rho C_p)_f} MEcf'^2 = 0, \tag{9}$$

With the boundary conditions (BCs):

$$\begin{cases} f(0) = S, \quad \theta(0) = 0, \\ \dfrac{\mu_{hnf}}{\mu_f}\left(1+\dfrac{1}{\beta}\right) f''(0) + CMa \text{ at } \eta = 0, \\ f'(\infty) \to 0, \quad \theta(\infty) \to 0 \quad \text{as} \quad \eta \to \infty. \end{cases} \tag{10}$$

The magnetic parameter $M = \left(\frac{\sigma_f B_0^2}{a\rho_f}\right)$, Modified Hartmann number $q = \left(\frac{\pi_o J_o M_o}{8a^2 \rho_f l}\right)$, Modified Brinkmann number $d = \left(\sqrt{\frac{v_f}{a}}\right)$, Non-dimensional number $\eta = \left(y\sqrt{\frac{a}{v_f}}\right)$, Radiation parameter $Rd = \left(\frac{4\sigma T_\infty^2}{kk_f}\right)$, Eckert number $Ec = \left(\frac{u_w^2}{C_p(T_w - T_\infty)}\right)$, Porous medium $K = \left(\frac{v_f}{ak}\right)$, Darcy-Forchheimer number $Fr = \left(\frac{C_b}{\sqrt{k}}\right)$, Prandtl number $Pr = \left(\frac{(C_p\mu)_f}{k_f}\right)$, Heat source/sink parameter $Q = \left(\frac{Q_o}{a(\rho C_p)_f}\right)$, Marangoni number $Ma = \left(\frac{\delta_o \gamma_f T_0}{l^2 a\sqrt{a\mu_f \rho_f}}\right)$, Casson Parameter $\beta_o = \left(1+\frac{1}{\beta}\right)$, surface movement parameter C, amount of nanoparticles Aluminium (Al_2O_3), and copper (ϕ_2) nanoparticles, and suction parameter S are important regulating factors.

Table 1. The scientific estimates for base fluid and nanoparticles [54, 55].

Property	Al_2O_3	Cu	H_2O
k (W/mK)	40	400	0.613
ρ (kg/m^3)	3970	8933	997.1
β (1/K)	0.85×10^{-5}	1.67×10^{-5}	21×10^{-5}
C_p (J/kgK)	765	385	4179
P_r	6.2		

Engineering quantities

$$C_{f_x} = \frac{\tau_w}{\rho_f u_w^2} \text{ where } \tau_w = \mu\left(\frac{\partial u}{\partial y}\right)_{y=0}, \quad Nu_x = \frac{xq_w}{k_f(T_w - T_\infty)} + (q_r)_{y=0} \quad \text{where } q_w = -k\left(\frac{\partial T}{\partial y}\right)_{y=0}, \tag{11}$$

The non-dimensionalized expression for C_{f_x} and Nu_x takes the following form:

$$C_{f_x} R_{e_x}^{1/2} = \frac{\mu_{hnf}}{\mu_f}\left(1+\frac{1}{\beta}\right) f''(0), \quad Nu_x R_{e_x}^{-1/2} = -\frac{k_{hnf}}{k_f}\left(1+\frac{4}{3}Rd\right)\theta'(0), \quad \text{where } R_{e_x}^{\frac{1}{2}} = x\left(\frac{a}{\nu}\right)^{\frac{1}{2}}. \tag{12}$$

3 Research Methodology

The thermophysical properties of the base fluid (water) and nanoparticles (Al_2O_3 and Cu) used in this study

Table 2. Aldhafeeri, Wahid, and Ahmad et al. [51–53] mathematical calculations for the thermophysical properties of HNFs.

Property	Formula
Thermal conductivity	$\frac{k_{hnf}}{k_f} = \frac{\frac{\phi_{s1}k_{s1}+\phi_{s2}k_{s2}}{\phi_{hnf}} + 2k_f + 2(\phi_{s1}k_{s1} + \phi_{s2}k_{s2}) - 2k_f\phi_{hnf}}{\frac{\phi_{s1}k_{s1}+\phi_{s2}k_{s2}}{\phi_{hnf}} + 2k_f + (\phi_{s1}k_{s1} + \phi_{s2}k_{s2}) - k_f\phi_{hnf}}$
Density	$\rho_{hnf} = \rho_{s1}\phi_1 + \rho_{s2}\phi_2 + \rho_f(1-\phi_{hnf})$, where $\phi_{hnf} = \phi_1 + \phi_2$
Heat capacity	$(\rho C_p)_{hnf} = (1-\phi_{hnf})(\rho C_p)_f + \phi_{s1}(\rho C_p)_{s1} + \phi_{s2}(\rho C_p)_{s2}$
Thermal expansion	$\beta_{hnf} = \frac{1}{\rho_{hnf}}(\phi_1\rho_{s1}\beta_{s1} + \phi_2\rho_{s2}\beta_{s2} + (1-\phi_{hnf})\rho_f\beta_f)$
Dynamic viscosity	$\frac{\mu_{hnf}}{\mu_f} = \frac{1}{(1-\phi_{hnf})^{2.5}}$

are presented in Table 1, while the mathematical expressions for hybrid nanofluid properties, including density, heat capacity, thermal conductivity, thermal expansion, and dynamic viscosity, are provided in Table 2.

This paper provides a mathematical expression of the governing equations for steady flow with heat transfer over a surface throughout an extended sheet. Similarity variables must be included in order to reduce a system of PDEs to ODEs. However, due to the highly nonlinear and interconnected nature of equations (8) and (9), as well as the linked BCs in equation (10), an explicit analytical approach is not feasible. For this reason, a strong numerical approach is used to solve this problem.

The built-in MATLAB solver `bvp4c`, which employs a finite-difference method with collocation, is utilized in this study owing to its accuracy and reliability for fourth-order nonlinear BVPs. Figure 2 illustrates the detailed flowchart of the `bvp4c` implementation procedure adopted in the present numerical scheme.

The bvp4c built-in MATLAB solver, which solves boundary value problems using a finite-difference approach, is often suggested among the possibilities because of its precision and dependability while handling fourth-order problems. This solution makes it possible to handle the changed equations effectively and is ideally suited for the current situation [48–50]. The processes for adding the bvp4c solver to the physical model are outlined in the following stages.

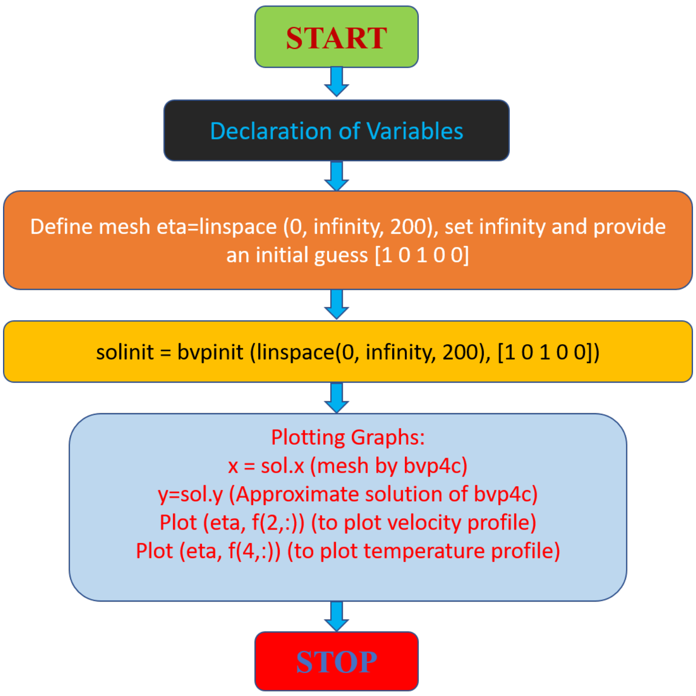

Figure 2. Bvp4c flow chart.

STEP 1: In Eqs. (8) and (9), higher order nonlinear ODEs are adjusted to account for recently included variables in the model.

$$f = y_1, \quad f' = y_2, \quad f'' = y_3, \quad \theta = y_4, \quad \theta' = y_5 \tag{13}$$

STEP 2: In Eqs. (8) and (9), utilize the further variables from Eq. (13) to decrease the higher-order

Table 3. Values of $Nu_x Re_x^{-\frac{1}{2}}$ when $\phi_1 = \phi_2 = 0.01$.

K	Ma	β_0	Rd	S	C	$Nu_x Re_x^{-\frac{1}{2}}$ (Hybrid Nanofluid)	$Nu_x Re_x^{-\frac{1}{2}}$ (Nanofluid)
0.2	0.2	0.2	0.2	0.2	1.0	14.009782	14.295171
0.3	—	—	—	—	—	13.870774	14.150342
0.4	—	—	—	—	—	13.738247	14.012345
0.5	—	—	—	—	—	13.611956	13.880919
—	0.3	—	—	—	—	15.427228	15.754096
—	0.4	—	—	—	—	16.559795	16.919330
—	0.5	—	—	—	—	17.518003	17.904917
—	—	0.3	—	—	—	13.349670	13.618335
—	—	0.4	—	—	—	12.895195	13.152300
—	—	0.5	—	—	—	12.551110	12.799480
—	—	—	0.3	—	—	12.629078	12.875490
—	—	—	0.4	—	—	12.175654	12.402732
—	—	—	0.5	—	—	12.108929	12.325219
—	—	—	—	0.3	—	16.644190	16.945664
—	—	—	—	0.4	—	19.481202	19.799251
—	—	—	—	0.5	—	22.477769	22.813537
—	—	—	—	—	1.1	14.325277	14.619966
—	—	—	—	—	1.2	14.622588	14.926002
—	—	—	—	—	1.3	14.904119	15.215765

nonlinear ODE system to a 1^{st} order nonlinear ODE system.

$$\begin{cases} f' = y_2, \\ f'' = y_3, \\ yy_1 = \dfrac{y_2 y_2 - y_1 y_3 - \dfrac{q}{A_2}\exp(-d\eta) + \dfrac{A_1}{A_2} K y_2 + Fr\, y_2 y_2}{A_1/A_2\left(1 + \dfrac{1}{\beta}\right)} \\ \theta' = y_5 \\ yy_2 = \dfrac{2y_2 y_4 - y_1 y_5 - \dfrac{Q}{A_5} y_4 - \dfrac{A_4}{A_5} MEc\, y_2 y_2}{\dfrac{A_3}{Pr\, A_5} + \dfrac{4Rd}{3Pr\, A_5}} \end{cases}$$

STEP 3: According to Eq. (10), boundary conditions must be specified using the newly supplied variables from Eq. (13).

$$\begin{cases} y_a(1) - S, \quad y_a(4), \quad A_1\left(1 + \dfrac{1}{\beta}\right) y_a(2) + CMa, \\ y_b(1), \quad y_b(4) \end{cases} \tag{14}$$

The values indicate the places on the sheet indicated by the subscripts a and b at $\eta = 0$, as well as the distance from the stretched sheet for a given value of η.

STEP 4: In the bvp4c solver, enter the boundary condition in Eq. (10) and the coupled of 1^{st} order nonlinear ODEs in Eqs. (8)-(9). As indicated by Eqs. (8) and (9), the structure of the algorithm *sol = bvp4c*

Table 4. Values of $-\theta'(0)$ when $\phi_1 = \phi_2 = 0.01$.

K	Ma	β_0	Rd	S	C	$-\theta'(0)$ (Nano fluid)	$-\theta'(0)$ (Hybrid Nanofluid)
0.2	0.2	0.2	0.2	0.2	1.0	11.419917	11.305967
0.3	—	—	—	—	—	11.304218	11.193787
0.4	—	—	—	—	—	11.193977	11.086837
—	0.3	—	—	—	—	12.585402	12.449854
—	0.4	—	—	—	—	13.516266	13.363841
—	—	0.3	—	—	—	10.879216	10.773254
—	—	0.4	—	—	—	10.506917	10.406489
—	—	—	0.3	—	—	9.295653	9.201630
—	—	—	0.4	—	—	8.168064	8.085751
—	—	—	—	0.3	—	13.537304	13.431948
—	—	—	—	0.4	—	15.816936	15.721432
—	—	—	—	—	1.1	11.679384	11.560574
—	—	—	—	—	1.2	11.923866	11.800505

(@ODEBVP, @ODEBC, Solinit, Options) including instruction for controlling the @ODEBVP function and @ODEBC, where @ODEBC is subject to the assumed boundary conditions of Eq. (10). Solinit describes the initial guess response. To better clarify the places where the borders criteria in @ODEBC are respected, a first approximation approach is developed using the ODEinit parameter in bvp4c. The solver's output is displayed as graphs and numerical solutions.

4 Results & Discussions

The steady MHD flow was examined numerically by solving the mathematical equations in (8)-(9) and (10) using the MATLAB program's boundary value problem solver (bvp4c) software. For the parameters Ma, S, ϕ_1, and ϕ_2, the boundary layer depth for the speed of heat exchange was 5, and for factor M, it ranged from 0 to 3. Table 2 represents the mathematical calculations for the thermophysical properties of HNFs, while Table 1 represents the scientific estimates for base fluid and nanoparticles. Table 3 shows the comparison of numerical results with previous studies. Tables 4, 5, 6 display the tabular and patterned numerical data for skin friction coefficient and Nusselt number. The values of Pr, which represents the flow's base fluid, was kept constant at 6.2 throughout the investigation. The performance of hybrid nanofluid flow applied to existing modeling was thoroughly examined by looking into the extra impacts of physical parameters M, Ma, S, ϕ_1, and ϕ_2.

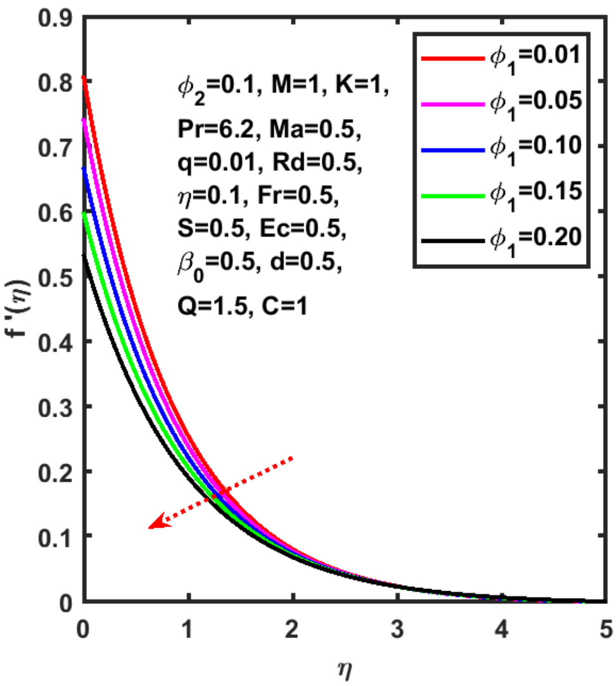

Figure 3. Impact of ϕ_1 on $f'(\eta)$.

Table 5. $Nu_x Re_x^{-\frac{1}{2}}$ values when $Pr = 0.62,\ Ma = 1,\ C = 1,\ \theta_0 = 0.1,\ M = K = S = 0$.

ϕ_1	ϕ_2	$Nu_x Re_x^{-\frac{1}{2}}$
0.001	0	14.298116
0.01	—	13.963529
0.10	—	10.936393
0.12	—	10.337224
0.13	—	10.046998
0.15	—	9.484739
0	0.001	14.301291
—	0.05	12.690214
—	0.01	13.994628
—	0.10	11.187689
—	0.12	10.624418
—	0.13	10.350559
—	0.15	9.818020

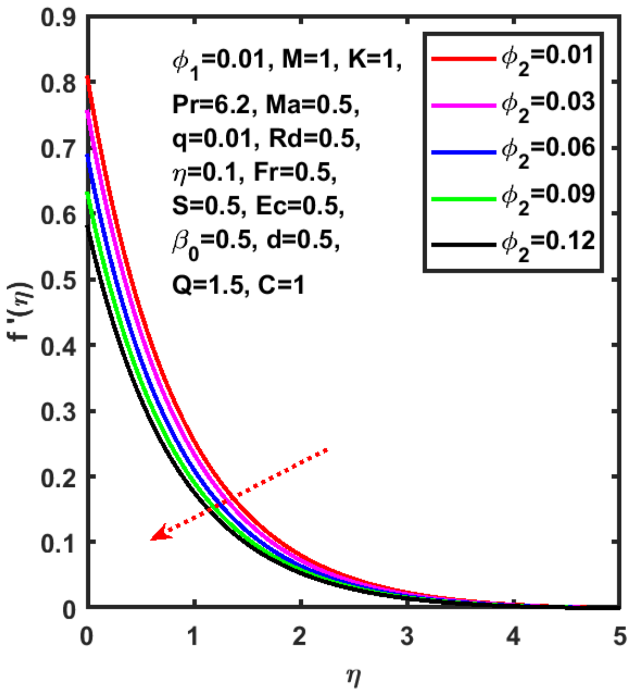

Figure 5. Impact of ϕ_2 on $f'(\eta)$.

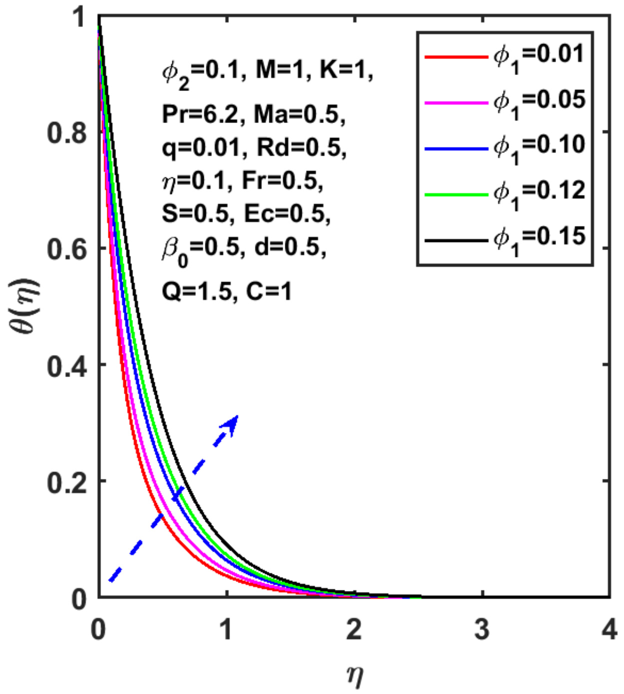

Figure 4. Impact of ϕ_1 on $\theta(\eta)$.

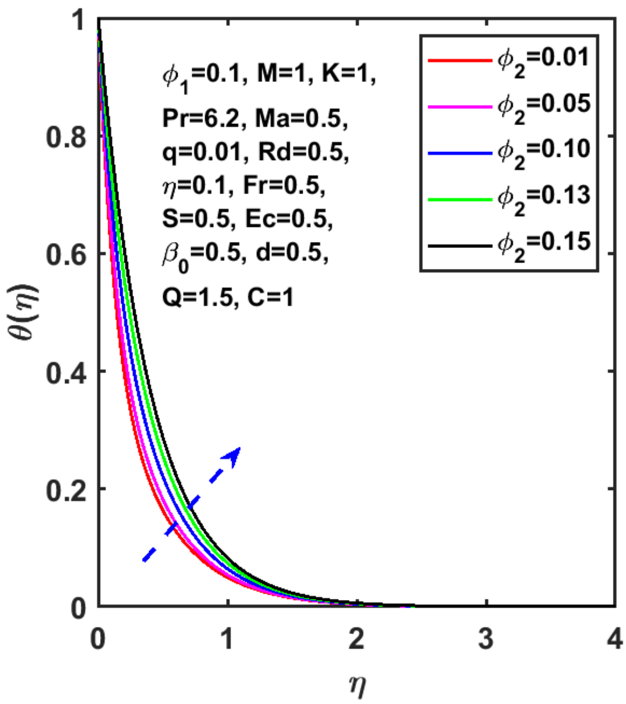

Figure 6. Impact of ϕ_2 on $\theta(\eta)$.

Figures 3 and 4 show the effect of the aluminum volumetric fraction (ϕ_1) on the velocity and temperature profiles. Increasing (ϕ_1) leads to a decrease in both the velocity and temperature distributions. While alumina nanoparticles enhance

Table 6. Comparison result with previous study.

M	$-\theta'(0)$		
	Current results	Abbas et al. [56]	Iqbal et al. [57]
0.3	0.8086334753	0.8086338914	0.8086332783
0.7	1.0000056168	1.0000063289	1.0000063001

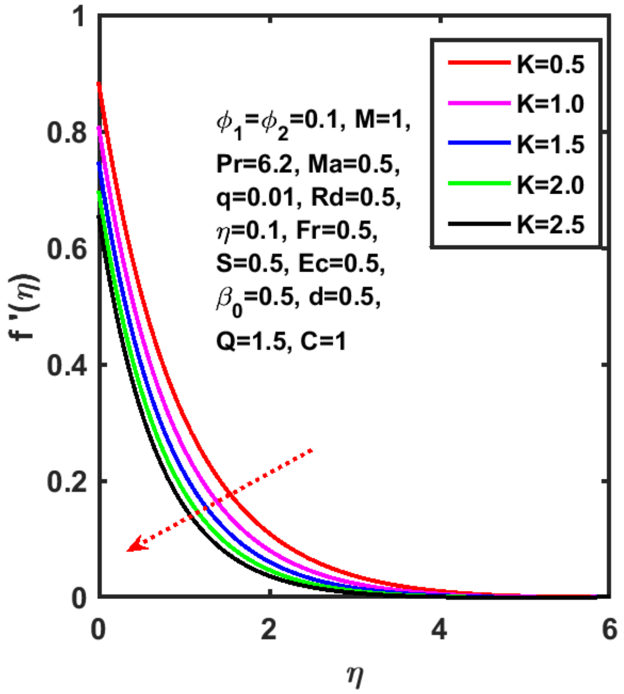

Figure 7. Effect of K on $f'(\eta)$.

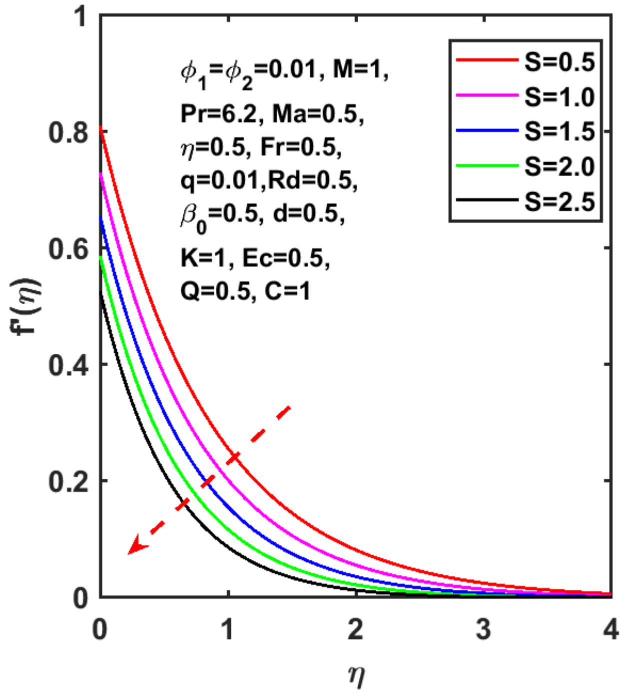

Figure 9. Effect of S on $f'(\eta)$.

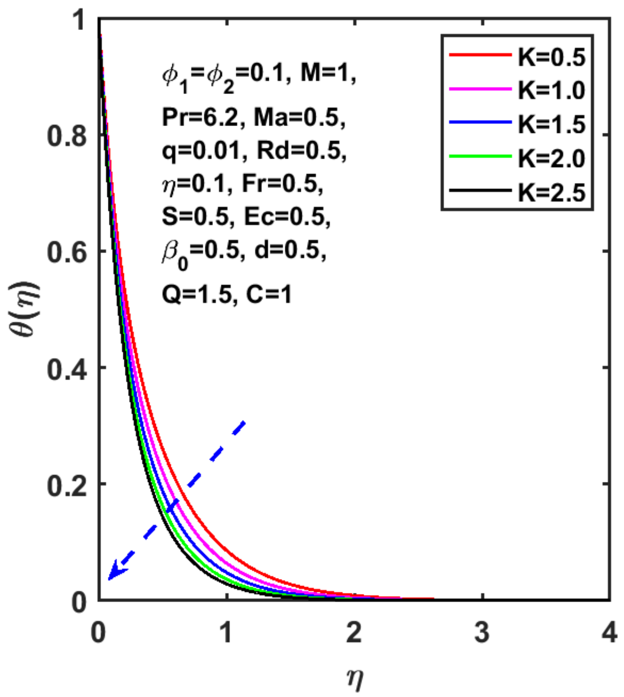

Figure 8. Impact of K on $\theta(\eta)$.

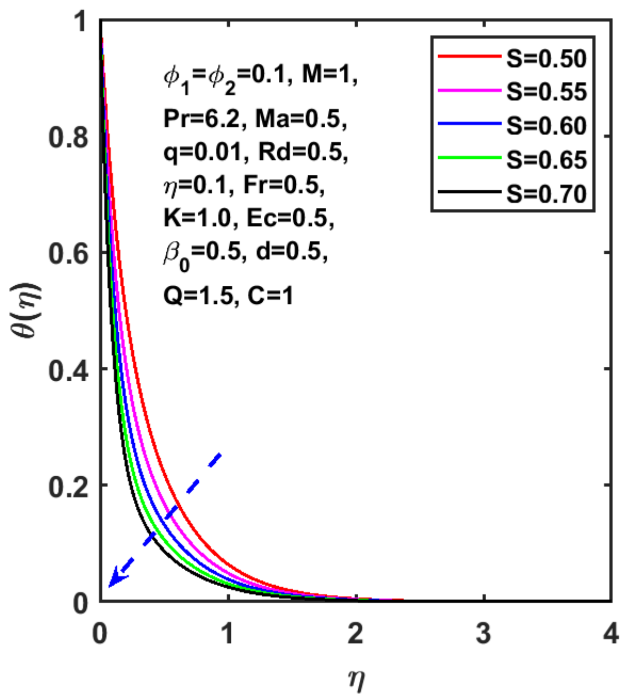

Figure 10. Impact of S on $\theta(\eta)$.

thermal conductivity, they also increase the dynamic viscosity of the hybrid nanofluid. The dominant viscous effect impedes fluid motion, thereby reducing momentum transfer. Consequently, the reduced flow leads to a thinner thermal boundary layer and a lower temperature profile.

Figures 5 and 6 show that while raising the volumetric percentage of aluminum oxide (ϕ_2) might somewhat increase thermal conductivity, this advantage may be offset by an increase in viscosity. Because the solid-liquid interfacial resistance increases when nanoparticles are added, the total thermal conductivity of the nanofluid may drop. Consequently, heat

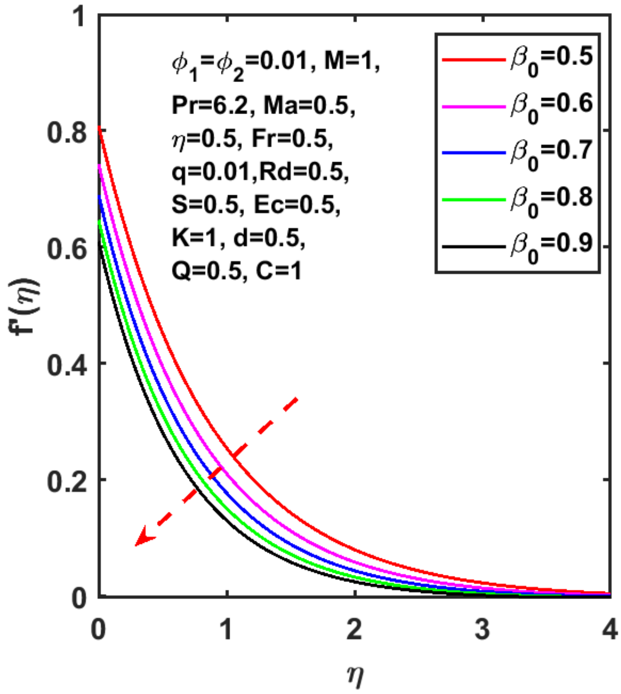

Figure 11. Impact of β_0 on $f'(\eta)$.

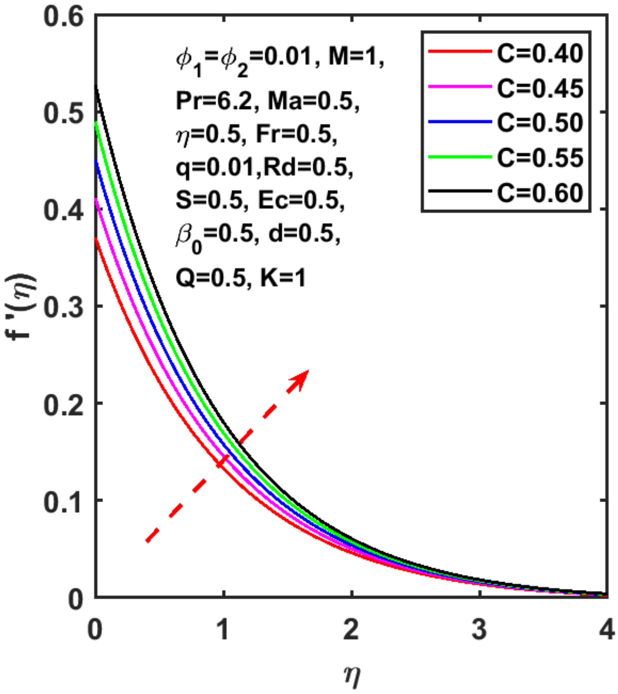

Figure 13. Influence of C on $f'(\eta)$.

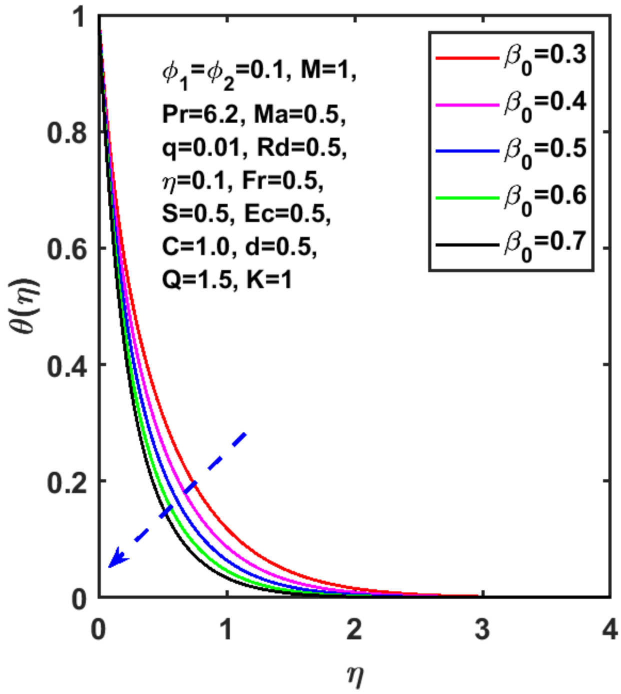

Figure 12. Effect of β_0 on $\theta(\eta)$.

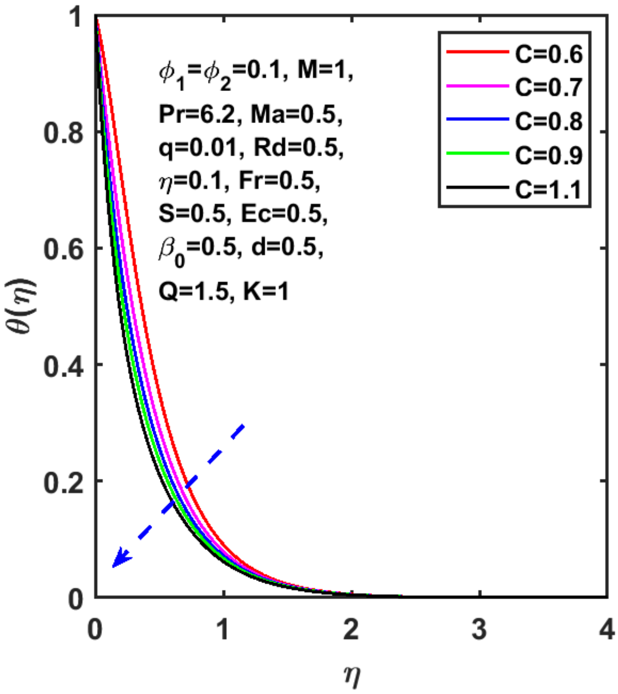

Figure 14. Surface movement C on $\theta(\eta)$.

transport through the fluid may become less efficient. This result implies that the benefits of adding nanoparticles in terms of thermal performance must be carefully weighed against the drawbacks of higher flow resistance. This observation's dependability is confirmed by several numerical studies, which also demonstrate its applicability in a variety of parameter ranges and modeling settings.

Figure 7 shows that velocity curve is impacted by the permeability component K in the porous substance. A rise in K causes the velocity curve to noticeably decrease. This phenomenon is explained by the porous medium's increased flow resistance. By increasing

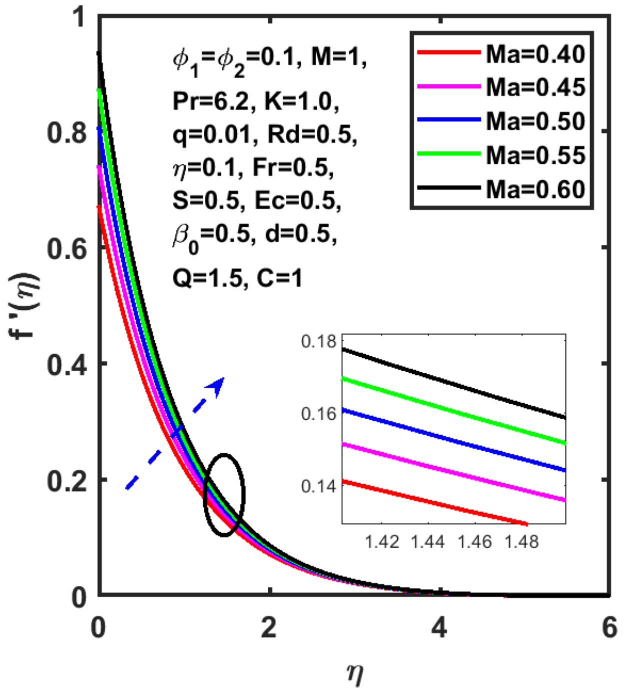

Figure 15. Impact of Ma on $f'(\eta)$.

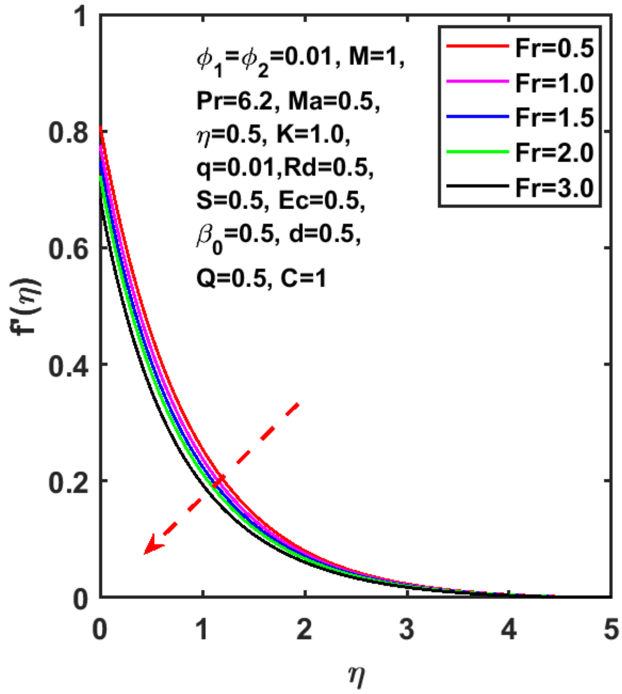

Figure 17. Impact of Fr on $f'(\eta)$.

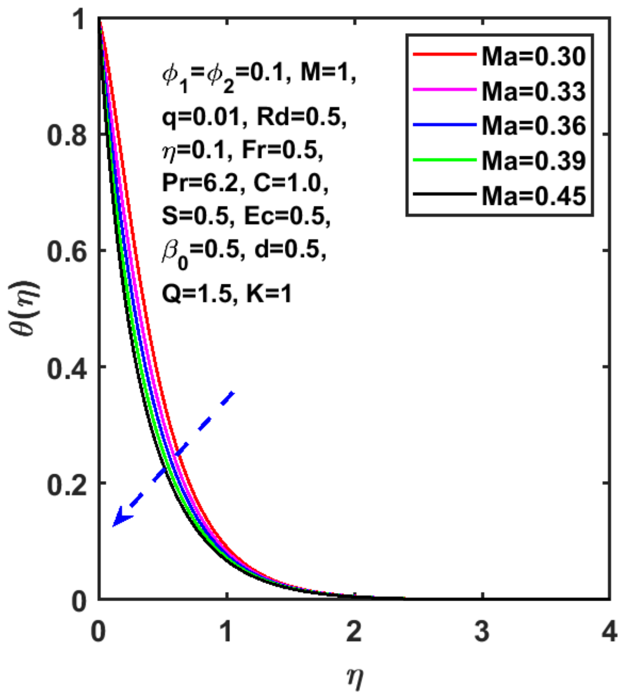

Figure 16. Impact of Ma on $\theta(\eta)$.

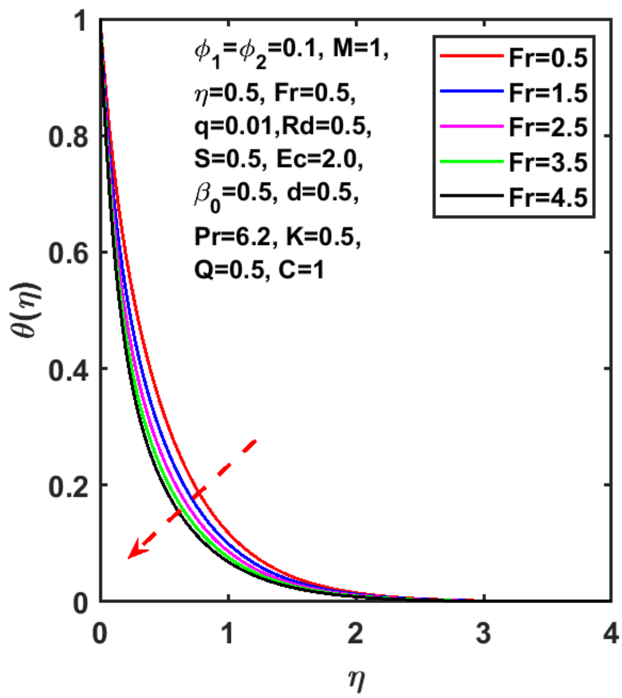

Figure 18. Impact of Ma on $\theta(\eta)$.

drag and internal friction, a denser or more resistant porous structure with a greater permeability value limits fluid mobility. The fluid's momentum decreases as a result, and the boundary layer gets thinner. Multiple simulations consistently support this pattern, demonstrating the accuracy of porous media effects in nanofluid flow modeling and establishing the dependability of the numerical results.

Figure 8 illustrates how the permeability variable K of the porous medium affects the temperature pattern inside the boundary layer. The temperature curve shows a discernible drop as K increases. This decrease is mostly caused by the porous medium's

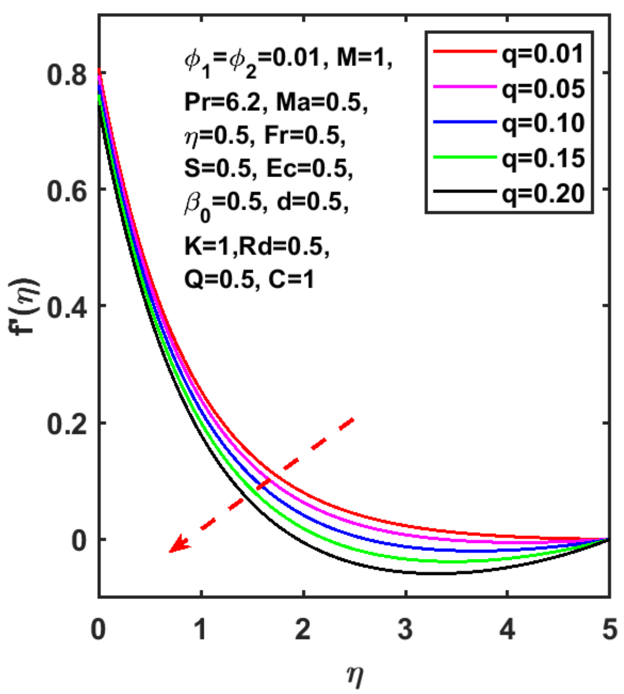

Figure 19. Impact of q on $f'(\eta)$.

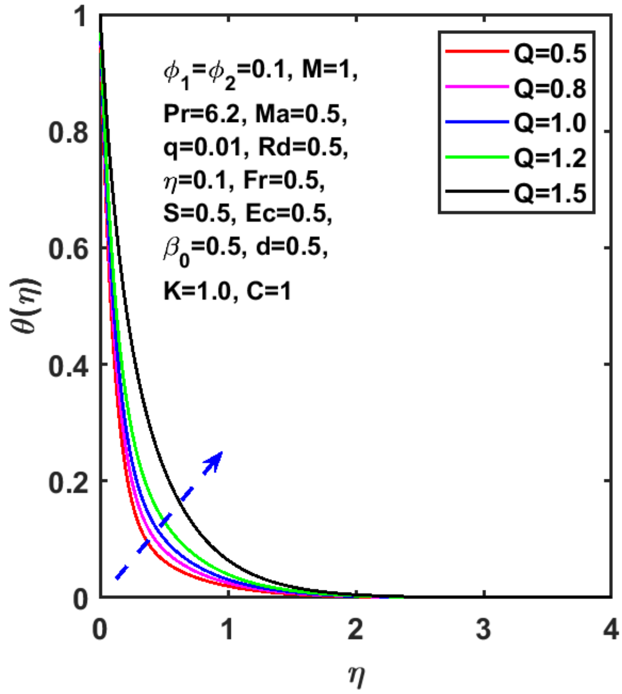

Figure 21. Effect of Q on $\theta(\eta)$.

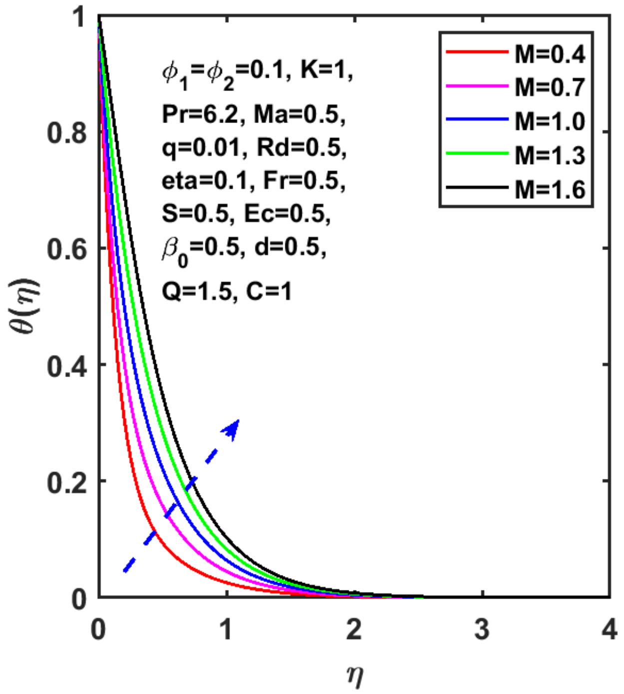

Figure 20. Effect of M on $\theta(\eta)$.

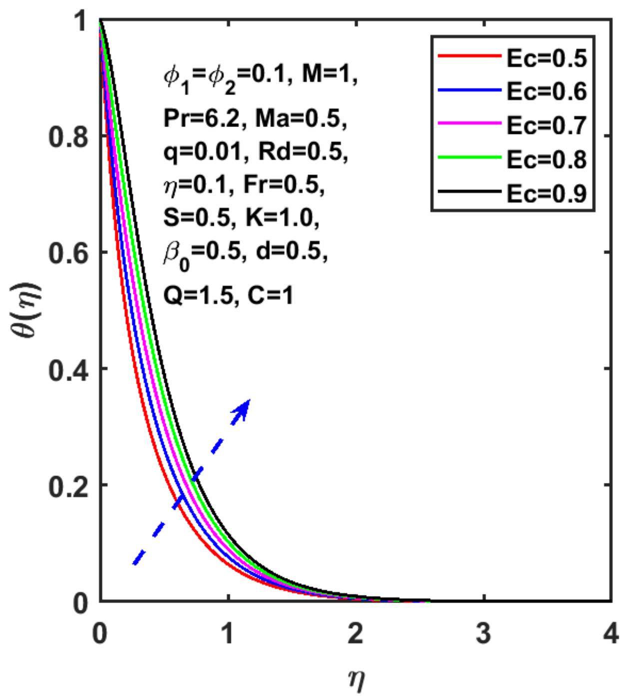

Figure 22. Impact of Ec on $\theta(\eta)$.

increased resistance, which limits thermal energy transmission in addition to fluid mobility. The increased drag causes the fluid to slow down, lowering the temperature across the boundary layer and delaying the convective heat transfer process. Numerical results have repeatedly confirmed this pattern, confirming the precision and dependability of the thermal behavior anticipated under various porosity circumstances. These discoveries are essential for improving thermal systems using nanofluids in porous materials.

Figure 9 illustrates how the velocity patterns is influenced by the suction factor S. The velocity across

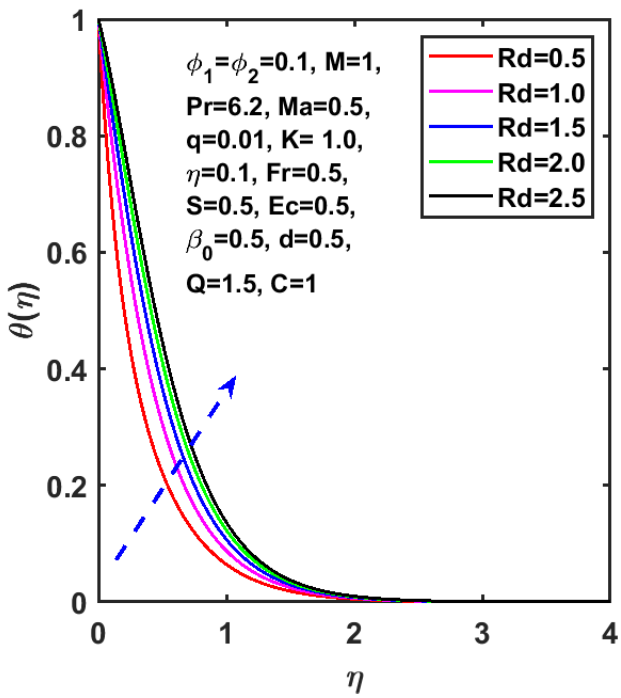

Figure 23. Impact of Rd on $\theta(\eta)$.

the boundary layer clearly decreases as the suction factor rises. Higher suction physically translates into fluid being withdrawn through the surface, which inhibits the formation of the boundary layer and attracts fluid particles to the sheet. This inward motion dampens the fluid momentum, lowering the overall velocity. A greater velocity gradient close to the surface is the result of suction-induced boundary layer thinning. Numerical study has reliably confirmed this behavior, guaranteeing the stability of the observed trend and validating the stabilizing impact of suction in flow control applications.

Figure 10 illustrates that the suction variable S affects the temperature distribution. There is a discernible drop in temperature within the BL as suction rises. This happens because the fluid is drawn toward the surface by suction, which thins the TBL and extracts hot fluid molecules. The temperature decreases as a result of less thermal energy being kept close to the surface. Furthermore, heat absorption is limited by the shorter residence period of fluid particles close to the heated surface. This steady pattern, shown in several simulations, demonstrates the value of suction's contribution to improving cooling and thermal boundary layer management in nanofluid applications and validates the accuracy of the thermal behavior linked to it.

Figure 11 illustrates that the Casson variable β_0 affects the velocity pattern. With increasing Casson variable, there is a noticeable drop in velocity over the boundary layer. The Casson fluid model characterizes non-Newtonian fluids as possessing yield stress, which denotes that the fluid resists motion until a certain stress threshold is crossed. Stronger yield stress behavior, which raises the fluid's flow resistance, is correlated with a higher Casson value. The fluid's momentum is decreased by this extra resistance, which slows the velocity profile and causes the boundary layer to contract. Numerical studies consistently support the trend, strengthening the observation's dependability and emphasizing the importance of the Casson parameter in simulating complicated fluids such as hybrid or ternary nanofluids.

Figure 12 illustrates that the Casson parameter β_0 affects the temperature curve. There is a noticeable drop in temperature within the thermal BL as the Casson component rises. This is because the fluid's ability to convey heat energy and movement is reduced due to its increased yield stress. The temperature across the boundary layer drops as the resistance to deformation rises because convective heat transmission is less efficient. This decrease suggests that Casson-type fluids subjected to severe non-Newtonian influences have less thermal diffusion. This pattern is confirmed by repeated simulations, which also highlight the importance of the Casson parameter in regulating the thermal properties of nanofluids in engineering applications.

Figures 13 and 14 demonstrate the velocity profile noticeably rises as the surface movement parameter (C) increases, suggesting that the fluid layers get more momentum from the increased surface stretching or motion. This increased momentum speeds up the fluid flow near the surface. However, the fluid's capacity to store heat is diminished by this broader range, leading to the compression of the thermal boundary layer. The temperature profile drops as C increases, indicating an inverse connection between flow field surface movement and thermal dispersion.

Figures 15 and 16 illustrate that the Marangoni convection variable affects patterns of temperature and velocity. The temperature curve clearly drops as the Marangoni variable rises, but the velocity curve rapidly rises as well. This action, which results in the fluid moving, is caused by the surface tension gradient that temperature changes along the fluid contact induce. Increased fluid velocity close to the interface results from improved surface-driven flow caused by stronger

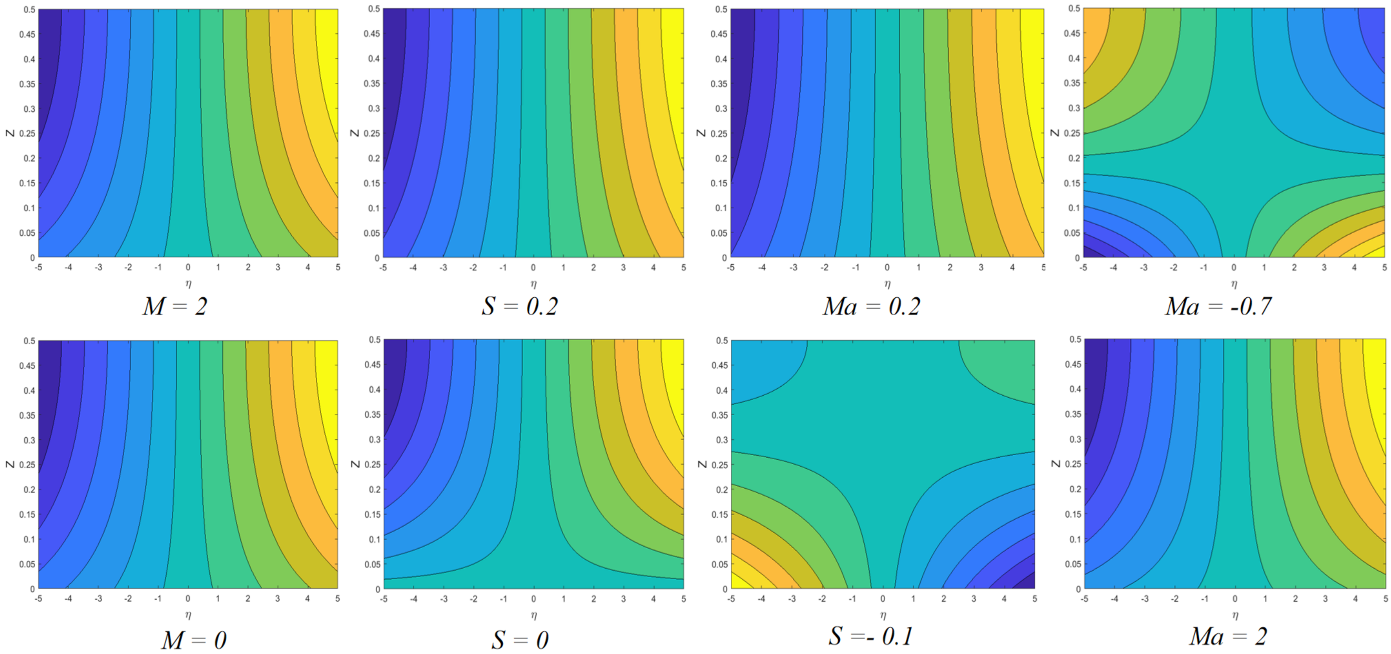

Figure 24. Streamlines for various values of the Magnetic, Suction, Marangoni parameters.

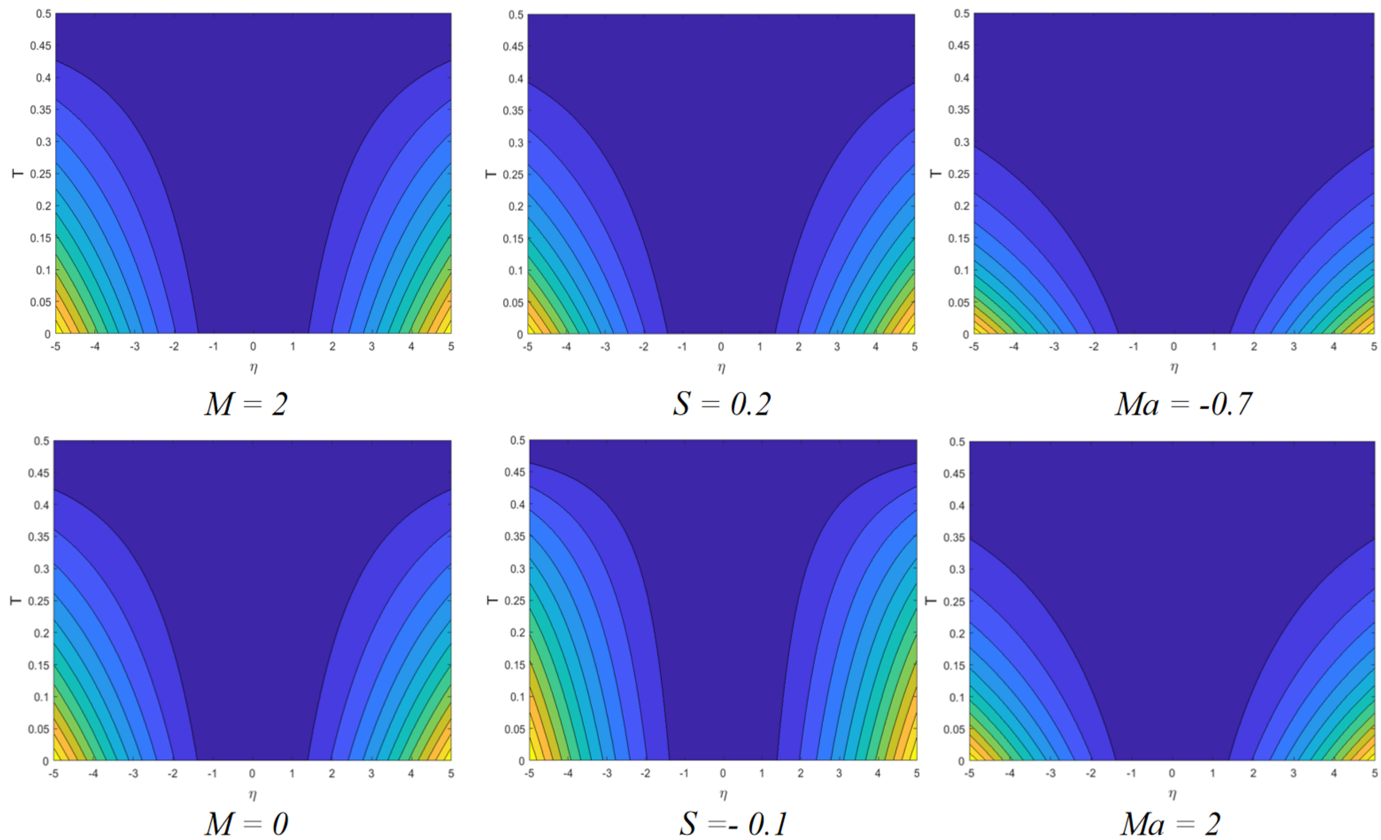

Figure 25. Isotherms for various values of the Magnetic, Suction, Marangoni parameters.

Marangoni convection. The thermal boundary layer shrinks and the temperature drops as a result of the enhanced mobility speeding up thermal transport away from the heated region.

Figures 17 and 18 demonstrate the influence of the Darcy–Forchheimer variable on the velocity and temperature distributions. As this parameter increases, the temperature and velocity profiles show a tendency to decline. The resistance caused by inertial effects and porous material inside the flow is represented by the Darcy–Forchheimer term. Elevated values of this parameter indicate greater resistance to fluid motion, resulting in reduced velocity. Because of this higher resistance, which also limits the convective flow of heat, the temperature within the boundary layer decreases. The dampening effect of inertial forces and porous drag is confirmed by the temperature and velocity drops occurring simultaneously. The regular validation of these patterns by numerical simulations demonstrates the accuracy and significance of Darcy–Forchheimer effects in forecasting nanofluid flow through porous materials.

Figure 19 shows a declining tendency as the modified Hartmann number rises. This happens when the magnetic field interacts with the electrically conducting fluid, increasing the Lorentz force. The Lorentz force, which acts as a resistive drag and opposes fluid motion, lowers the flow velocity. The fluid moves more slowly over the boundary layer due to this magnetic damping effect, which is exacerbated by higher Hartmann numbers. A few magnetic limitation estimations M with magnetic nanoparticles in the regular fluid are shown in the Figure 20 along with the temperature field change. As the magnetic value M rises, the temperature curve falls because the thermal boundary layer gets thinner.

Figure 21 illustrates that the temperature curve noticeably rises as the heat production component Q is raised. This is because greater Q values point to more fluid heat production, which instantly raises the thermal energy of the system. In addition to, the temperature of the boundary layer increases and the thermal gradient becomes more apparent. The consistency of this pattern in simulations shows that the model can properly represent the effect of internal heat sources on the temperature distribution of hybrid nanofluids.

Figure 22 demonstrates that a temperature curve is affected by an Eckert number E_c. The thermal boundary layer gets thicker as its temperature increases. Considering that Eckert's is the ratio of boundary layer enthalpy modification to dynamic energy flow, this temperature increase is logically the outcome of an inferior enthalpy variance. It speeds up the process of kinetic energy being converted to internal energy by changing fluid tensions.

The radiation factor R_d has an impact on the temperature curve, as shown in Figure 23. The increased heat transmission of radiation between the sheet and its surroundings is shown by the increase in the linear radiation variable. The temperature distribution over the surface may drop as a result of this improved radiation heat transfer as heat is being radiated away more efficiently.

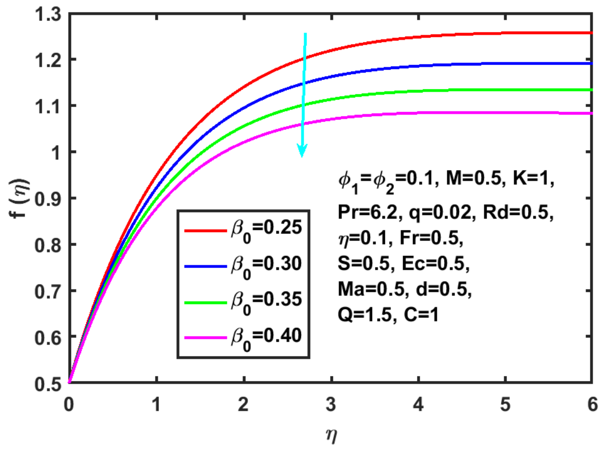

Figure 26. Aspect of β_0 on $\theta(\eta)$.

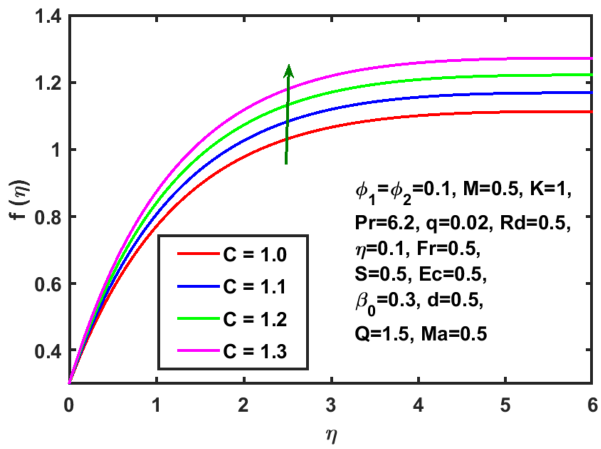

Figure 27. Aspect of C on $f(\eta)$.

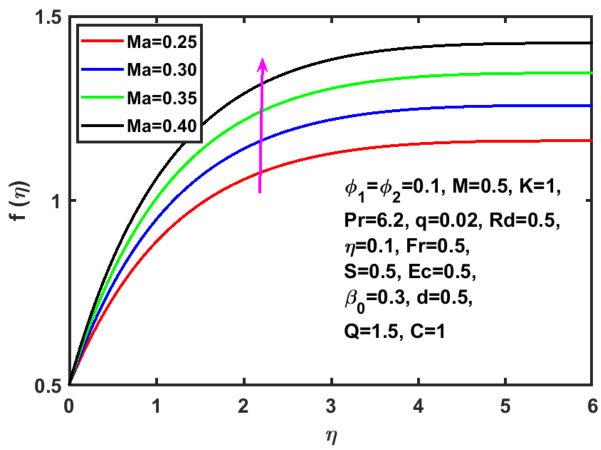

Figure 28. Aspect of Ma on $f(\eta)$.

Figure 24 shows the stream lines for various values of magnetic field, Marangoni convection, while for these parameters the Isotherms also plotted as shown in Figures 25. Figures 26, 27, 28 show the graphs of $f(\eta)$ for various values of Casson, magnetic, and surface movement parameters.

5 Conclusion

The purpose of this research is to examine magnetized flow of hybrid nanofluids is affected by suction, Casson fluid, joule heating, thermal radiation, and Darcy-Forchheimer in the form of nanoparticles and a stretching/shrinking sheet caused by a Riga plate. The computational findings are obtained using MATLAB's built-in Bvp4c function. This study advances our knowledge of heat transfer mechanisms and hybrid nanofluid dynamics, which may find use in energy systems and thermal management. The study's findings provide useful information for improving the efficiency and design of hybrid nanofluid systems, particularly in situations where suction, stretching/shrinking sheets, and Darcy-Forchheimer flow are crucial.

The following summarizes the investigation's main findings:

- The velocity and temperature figures both are decreases as the volume concentration of Al_2O_3 increases.
- The temperature curve increases and the velocity curve decreases as the volume concentration of Cu rises.
- Improved resistance to heat transmission and fluid motion is suggested by the simultaneous decrease in the temperature and velocity figures as the porous medium component rises.
- The suction parameter reduces the velocity profile while enhancing the Nusselt number by thinning the thermal boundary layer.
- The greater fluid resistance and lower thermal diffusion associated with non-Newtonian fluid behavior are shown by the temperature and velocity distributions decreasing as the Casson variable enhanced.
- More surface movement improves the velocity figure and reduces the temperature distribution because of lesser thermal boundary layers and more shear effects.
- As the Casson parameters increases, the velocity plot drops, but the temperature curves increase.
- The velocity distribution rises with an increase in the Marangoni convection variable, while the temperature curve falls, indicating stronger surface tension gradients that promote fluid motion and reduce thermal diffusion.
- As the Darcy–Forchheimer and Radiation parameter increases, both velocity and temperature distributions drop because of the higher flow resistance and less convective heat transfer inside the porous material.
- As the modified Hartmann number rises, the Lorentz force which opposes fluid motion-becomes greater, hence the velocity curve decreases.
- As the values of the magnetic field, heat generation/absorption, and Eckert number increase, the temperature profile rises significantly.

Data Availability Statement

Data will be made available on request.

Funding

This work was supported without any funding.

Conflicts of Interest

The authors declare no conflicts of interest.

AI Use Statement

The authors declare that no generative AI was used in the preparation of this manuscript.

Ethical Approval and Consent to Participate

Not applicable.

References

[1] Wahid, N. S., Arifin, N. M., Khashi'ie, N. S., & Pop, I. (2021). Marangoni hybrid nanofluid flow over a permeable infinite disk embedded in a porous medium. *International Communications in Heat and Mass Transfer, 126*, 105421. [CrossRef]

[2] Abbas, M., Khan, N., Hashmi, M. S., & Younis, J. (2023). Numerically analysis of Marangoni convective flow of hybrid nanofluid over an infinite disk with thermophoresis particle deposition. *Scientific Reports, 13*(1), 5036. [CrossRef]

[3] Elbashbeshy, E. M., Asker, H. G., & Saad, H. (2024). Heat transfer transmission in a Marangoni

boundary layer flow along an inclined disk in a porous medium. *Ain Shams Engineering Journal, 15*(1), 102228. [CrossRef]

[4] Agrawal, P., Dadheech, P. K., Jat, R., Nisar, K. S., Bohra, M., & Purohit, S. D. (2021). Magneto Marangoni flow of γ-AL2O3 nanofluids with thermal radiation and heat source/sink effects over a stretching surface embedded in porous medium. *Case Studies in Thermal Engineering, 23*, 100802. [CrossRef]

[5] Choi, S. U. (1995, November). Enhancing thermal conductivity of fluids with nanoparticles. In *ASME international mechanical engineering congress and exposition* (Vol. 17421, pp. 99-105). American Society of Mechanical Engineers. [CrossRef]

[6] Saqib, M., Khan, I., Shafie, S., & Qushairi, A. (2019). Recent advancement in thermophysical properties of nanofluids and hybrid nanofluids: an overview. *City Univ. Int. J. Comput. Anal, 3*(2), 16-25. [Link]

[7] Saidur, R., Leong, K. Y., & Mohammed, H. A. (2011). A review on applications and challenges of nanofluids. *Renewable and sustainable energy reviews, 15*(3), 1646-1668. [CrossRef]

[8] Sohail, M., Rafique, E., Singh, A., & Tulu, A. (2024). Engagement of modified heat and mass fluxes on thermally radiated boundary layer flow past over a stretched sheet via OHAM analysis. *Discover Applied Sciences, 6*(5), 240. [CrossRef]

[9] Jahnavi, K. R., & Hegde, G. S. (2024). A review on nano fluid production, mathematical modelling and applications. *Journal of Nanofluids, 13*(2), 269-305. [CrossRef]

[10] Zangooee, M. R., Hosseinzadeh, K., & Ganj, D. D. (2022). Investigation of three-dimensional hybrid nanofluid flow affected by nonuniform MHD over exponential stretching/shrinking plate. *Nonlinear Engineering, 11*(1), 143-155. [CrossRef]

[11] Waseem, F., Sohail, M., Lone, S. A., & Chambashi, G. (2023). Numerical simulations of heat generation, thermal radiation and thermal transport in water-based nanoparticles: OHAM study. *Scientific Reports, 13*(1), 15650. [CrossRef]

[12] Algehyne, E. A., Lone, S. A., Raizah, Z., Eldin, S. M., Saeed, A., & Galal, A. M. (2023). Analysis of the electrically conducting magnetohydrodynamic hybrid nanofluid flow past a convectively heated stretching surface with suction/injection and non-linear thermal radiation. *Frontiers in Materials, 10*, 1132124. [CrossRef]

[13] Huminic, G., & Huminic, A. (2018). Hybrid nanofluids for heat transfer applications–a state-of-the-art review. *International Journal of Heat and Mass Transfer, 125*, 82-103. [CrossRef]

[14] Sharma, R. P., Prakash, O., & Shafi, S. (2024). MHD hybrid nanofluid and slip flow towards an exponentially stretching/shrinking sheet with nonlinear thermal radiation and nonuniform heat source/sink. *Modern Physics Letters B, 38*(23), 2450195. [CrossRef]

[15] Dandu, S., Chitrapu, V. R. M., & Kodi, R. (2024). An investigation into the impact of thermal radiation and chemical reactions on the flow through porous media of a Casson hybrid nanofluid including unstable mixed convection with stretched sheet in the presence of thermophoresis and Brownian motion. *Open Physics, 22*(1), 20240043. [CrossRef]

[16] Abbas, M., Khan, N., Hashmi, M. S., & Inc, M. (2023). Numerical analysis of Marangoni convective flow of gyrotactic microorganisms in dusty Jeffrey hybrid nanofluid over a Riga plate with Soret and Dufour effects. *Journal of Thermal Analysis & Calorimetry, 148*(22), 12609-12627. [CrossRef]

[17] Turkyilmazoglu, M. (2025). Exact momentum layer and thermal field solutions for the fluid flow due to a moving/deforming Riga plate. *International Journal of Thermal Sciences, 208*, 109448. [CrossRef]

[18] Otman, H. A., Mahmood, Z., Khan, U., Eldin, S. M., Fadhl, B. M., & Makhdoum, B. M. (2023). Mathematical analysis of mixed convective stagnation point flow over extendable porous riga plate with aggregation and joule heating effects. *Heliyon, 9*(6). [CrossRef]

[19] Hussain, Z., Bashir, Z., & Anwar, M. S. (2025). Analysis of nanofluid flow subject to velocity slip and Joule heating over a nonlinear stretching Riga plate with varying thickness. *Waves in Random and Complex Media, 35*(6), 11789-11805. [CrossRef]

[20] Eldabe, N. T., Gabr, M. E., Zaher, A. Z., & Zaher, S. A. (2021). The effect of Joule heating and viscous dissipation on the boundary layer flow of a magnetohydrodynamics micropolar-nanofluid over a stretching vertical Riga plate. *Heat Transfer, 50*(5), 4788-4805. [CrossRef]

[21] Turkyilmazoglu, M. (2024). Two models on the unsteady heat and fluid flow induced by stretching or shrinking sheets and novel time-dependent solutions. *ASME Journal of Heat and Mass Transfer, 146*(10), 101802. [CrossRef]

[22] Jawad, M., Ghazwani, H. A., Ali, M. R., Hendy, A. S., Majeed, A. H., & Wang, X. (2023). Numerical simulation for thermal radiative flow of tangent hyperbolic nanofluid due to Riga plate in the presence of joule heating. *Case Studies in Thermal Engineering, 52*, 103686. [CrossRef]

[23] Eladeb, A., Sambas, A., Bilal, M., Alshammari, B. M., & Kolsi, L. (2025). Radiative Darcy-Forchheimer hybrid nanofluid flow with thermal and bioconvection impacts over a stretching/shrinking sheet. *Journal of Radiation Research and Applied Sciences, 18*(1), 101266. [CrossRef]

[24] Gautam, A. K., Verma, A. K., Bhattacharyya, K., Mukhopadhyay, S., & Chamkha, A. J. (2024). Impacts of activation energy and binary chemical

reaction on MHD flow of Williamson nanofluid in Darcy–Forchheimer porous medium: A case of expanding sheet of variable thickness. *Waves in Random and Complex Media, 34*(4), 3528-3549. [CrossRef]

[25] Ullah, Z., Zari, I., Gul, T., Ali, I., Alghamdi, W., & Ali, F. (2023). Darcy-Forchheimer hybrid nanofluids flow with quadratic convection over a stretched tube. *Advances in Mechanical Engineering, 15*(6), 16878132231180866. [CrossRef]

[26] Muhammad, T., Lu, D. C., Mahanthesh, B., Eid, M. R., Ramzan, M., & Dar, A. (2018). Significance of Darcy-Forchheimer porous medium in nanofluid through carbon nanotubes. *Communications in Theoretical Physics, 70*(3), 361. [CrossRef]

[27] Alqahtani, A. M., Bilal, M., Usman, M., Alsenani, T. R., Ali, A., & Mahmuod, S. R. (2023). Heat and mass transfer through MHD Darcy Forchheimer Casson hybrid nanofluid flow across an exponential stretching sheet. *ZAMM-Journal of Applied Mathematics and Mechanics/Zeitschrift für Angewandte Mathematik und Mechanik, 103*(6), e202200213. [CrossRef]

[28] Usman, M., Amin, S., & Saeed, A. (2022). Magnetohydrodynamic hybrid nanofluid flow with the effect of Darcy–Forchheimer theory and slip conditions over an exponential stretchable sheet. *Advances in Mechanical Engineering, 14*(8), 16878132221116479. [CrossRef]

[29] Rasool, G., Chamkha, A. J., Muhammad, T., Shafiq, A., & Khan, I. (2020). Darcy-Forchheimer relation in Casson type MHD nanofluid flow over non-linear stretching surface. *Propulsion and Power Research, 9*(2), 159-168. [CrossRef]

[30] Ali, F., Zaib, A., Abbas, M., Anitha, G., Loganathan, K., & Reddy, G. R. (2024). Radiative flow of cross ternary hybrid nanofluid (MoS2, TiO2, Ag/CMC-water) in a Darcy Forchheimer porous medium over a stretching cylinder with entropy minimization. *Heliyon, 10*(14). [CrossRef]

[31] Alkasasbeh, H. T. (2025). Modeling the flow of Casson nanofluid on a stretching sheet with heat transfer: a study of electric MHD and Darcy-Forchheimer effects. *Partial Differential Equations in Applied Mathematics, 13*, 101109. [CrossRef]

[32] Kaswan, P., Kumar, M., Kumari, M., Mandal, G., & Obalalu, A. M. (2025). Stability and multiple solutions of ternary hybrid nanofluid in a Darcy–Forchheimer porous medium over a stretching/shrinking surface. *Journal of Thermal Analysis and Calorimetry, 150*(13), 10575-10593. [CrossRef]

[33] Memon, M. A., Jacob, K., Lanjwani, H. B., & Mahmoud, E. E. (2024). Darcy-Forchheimer MHD micropolar water based hybrid nanofluid flow, heat and mass transfer features past on stretching/shrinking surface with slip and radiation effects. *Results in Engineering, 23*, 102534. [CrossRef]

[34] Saleem, M., Hussain, M., & Inc, M. (2023). Significance of Darcy–Forchheimer law and magnetic field on the comparison of Williamson–Casson fluid subject to an exponential stretching sheet. *International Journal of Modern Physics B, 37*(27), 2350315. [CrossRef]

[35] Jat, K., Sharma, K., Choudhary, P., Soni, P., Ali, R., & Ganesh, M. (2024). Significance of Darcy–Forchheimer Casson fluid flow past a non-permeable curved stretching sheet with the impacts of heat and mass transfer. *Case Studies in Thermal Engineering, 61*, 104907. [CrossRef]

[36] Sohail, M., Waseem, F., Abodayeh, K., & Rafique, E. (2026). Analysis of entropy generation on Darcy-Forchheimer squeezed hybrid nanofluid flow between two parallel rotating disks by considering thermal radiation and viscous dissipation. *Numerical Heat Transfer, Part B: Fundamentals, 87*(1), 2391501. [CrossRef]

[37] Sindhu, R., Eswaramoorthi, S., Loganathan, K., & Jain, R. (2024). Comparative approach of Darcy–Forchheimer flow on water based hybrid nanofluid (Cu-Al2O3) and mono nanofluid (Cu) over a stretched surface with injection/suction. *Partial Differential Equations in Applied Mathematics, 11*, 100786. [CrossRef]

[38] Zainal, N. A., Nazar, R., Naganthran, K., & Pop, I. (2021). Stability analysis of MHD hybrid nanofluid flow over a stretching/shrinking sheet with quadratic velocity. *Alexandria Engineering Journal, 60*(1), 915-926. [CrossRef]

[39] Jaafar, A. I., Jamaludin, A., Nazar, R., & Pop, I. (2023). MHD Marangoni convection heat transfer of Ag-Cu hybrid nanofluid under a stretching/shrinking sheet with the effect of suction. *International Journal of Modern Physics C, 34*(10), 2350134. [CrossRef]

[40] Zainal, N. A., Nazar, R., Naganthran, K., & Pop, I. (2021). Heat generation/absorption effect on MHD flow of hybrid nanofluid over bidirectional exponential stretching/shrinking sheet. Chinese Journal of Physics, 69, 118-133. [CrossRef]

[41] Shaikh, G. M., Memon, A. A., Memon, M. A., Yashkun, U., Obalalu, A. M., & Köten, H. (2024). Numerical study of flow behavior and heat transfer of ternary water-based nanofluids in the presence of suction/injection, stretching/shrinking sheet. *Journal of Thermal Engineering, 10*(4), 1021-1043. [Link]

[42] Maiti, H., & Mukhopadhyay, S. (2023). Existence of MHD boundary layer hybrid nanofluid flow through a divergent channel with mass suction and injection. *Chemical Engineering Journal Advances, 14*, 100475. [CrossRef]

[43] Khan, M. S., Mei, S., Shabnam, Ali Shah, N., Chung, J. D., Khan, A., & Shah, S. A. (2022). Steady squeezing flow of magnetohydrodynamics hybrid nanofluid flow comprising carbon nanotube-ferrous oxide/water with suction/injection effect. *Nanomaterials, 12*(4), 660.

[CrossRef]

[44] Gumber, P., Yaseen, M., Rawat, S. K., & Kumar, M. (2022). Heat transfer in micropolar hybrid nanofluid flow past a vertical plate in the presence of thermal radiation and suction/injection effects. *Partial Differential Equations in Applied Mathematics, 5*, 100240. [CrossRef]

[45] Gokulavani, P., Muthtamilselvan, M., & Abdalla, B. (2022). Impact of injection/suction and entropy generation of the porous open cavity with the hybrid nanofluid. *Journal of Thermal Analysis and Calorimetry, 147*(4), 3299-3313. [CrossRef]

[46] Khashi'Ie, N. S., Arifin, N. M., Pop, I., Nazar, R., Hafidzuddin, E. H., & Wahi, N. (2020). Thermal Marangoni flow past a permeable stretching/shrinking sheet in a hybrid Cu–Al. *Sains Malaysiana, 49*(1), 211-222. [CrossRef]

[47] Alabdulhadi, S., Waini, I., Ahmed, S. E., & Ishak, A. (2021). Hybrid nanofluid flow and heat transfer past an inclined surface. *Mathematics, 9*(24), 3176. [CrossRef]

[48] Shampine, L. F., Kierzenka, J., & Reichelt, M. W. (2000). Solving boundary value problems for ordinary differential equations in MATLAB with bvp4c. *Tutorial notes, 2000*, 1-27. [Link]

[49] Hale, N., & Moore, D. R. (2008, April). *A sixth-order extension to the MATLAB package bvp4c of J. Kierzenka and L. Shampine* (Report No. 08/04). Oxford University Computing Laboratory, Numerical Analysis Group. https://ora.ox.ac.uk/objects/uuid:8a565484-8be4-40a6-a5d3-b3d96d0e6859

[50] Esfandiari, R. S. (2017). *Numerical methods for engineers and scientists using MATLAB®*. Crc Press.

[51] Aldhafeeri, A. A., & Yasmin, H. (2024). A numerical analysis of the rotational flow of a hybrid nanofluid past a unidirectional extending surface with velocity and thermal slip conditions. *Reviews on Advanced Materials Science, 63*(1), 20240052. [CrossRef]

[52] Wahid, N. S., Arifin, N. M., Khashi'ie, N. S., Pop, I., Bachok, N., & Hafidzuddin, M. E. H. (2022). Unsteady mixed convective stagnation point flow of hybrid nanofluid in porous medium. *Neural Computing and Applications, 34*(17), 14699-14715. [CrossRef]

[53] Ahmad, W. (2026). Influence of Darcy-Forchheimer Effects on 3D MHD Rotating Flow of Casson Hybrid Nanofluid with Velocity Slip and Convective Boundary Conditions. *ICCK Journal of Applied Mathematics, 2*(1), 44-63. [CrossRef]

[54] Mahanthesh, B., Gireesha, B., & Gorla, R. S. R. (2016). Heat and mass transfer effects on the mixed convective flow of chemically reacting nanofluid past a moving/stationary vertical plate. *Alexandria engineering journal, 55*, 569-581. [CrossRef]

[55] Ahmad, W., Saqib, M., Khan, I., Oqilat, O., & Khan, M. S. (2025). Significance of Soret Dufour Effects on MHD mixed convective flow of maxwell hybrid nanofluid in porous medium with activation energy. *International Journal of Thermofluids, 28*, 101278. [CrossRef]

[56] Abbas, M., Akgül, A., Ibrahim, T. K., Al-Mdallal, Q., Turdialiyev, U., Ghazi, H. M., ... & Garalleh, H. A. (2025). Local thermal non-equilibrium effects on Marangoni convective flow of Casson fluid with elastic deformation: Perspective of Cattaneo-Christov flux model. *International Journal of Thermofluids, 27*, 101268. [CrossRef]

[57] Iqbal, M. A., Khan, N., Alhefthi, R. K., & Inc, M. (2025). Bio-convective flow of magnetized Casson fluid over a sheet in the presence of thermophoretic particle deposition and convective boundary conditions. *Modern Physics Letters B, 39*(12), 2450466. [CrossRef]

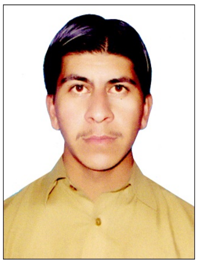

Waqas Ahmad received the M.Phil degree in Applied Mathematics from Qurtuba University of Science & Information Technology Peshawar, Pakistan. (Email: waqas64065@gmail.com)